Fusion Engineering and Design 112 (2016) 633–645

Contents lists available at ScienceDirect

Fusion Engineering and Design

journal homepage: www.elsevier.com/locate/fusengdes

Geometric formulas for system codes including the effect of negative triangularity

O. Sauter

Ecole Polytechnique Fédérale de Lausanne (EPFL), Swiss Plasma Center (SPC), CH-1015 Lausanne, Switzerland

HIGHLIGHTS

- New simple accurate formulas for geometric quantities for tokamak plasmas are given.
- The formulas are valid for both positive and negative triangularity.
- They are typically useful for DEMO and system codes studies.
- A formula for the trapped fraction is also given.

ARTICLE INFO

Article history:
Received 3 February 2016
Received in revised form 22 March 2016
Accepted 18 April 2016
Available online 25 May 2016

Keywords:
Tokamak
System codes
Equilibrium
DEMO

ABSTRACT

Formulas for the volume, poloidal and toroidal surfaces, poloidal length, plasma current, and hence average poloidal field, are determined using global parameters of tokamak plasmas. Previous formulas did not include systematically the effect of triangularity and in particular are inaccurate for negative triangularity cases. Since tokamaks with negative triangularity can be attractive for DEMO reactors [1,2], it is important to have updated formulas. It is also shown that the combined effect of finite triangularity and inverse aspect ratio was not correctly taken into account. Previous formulas were also using in some cases shaping parameters at the 95% poloidal flux surface. It is shown that this is misleading and the new formulas, including I_p and q_{95}, use the effective parameters, κ, δ, R_{geom}, ϵ of the relevant flux surface, in this case of the last closed flux surface. Only the value of the safety factor, q, is ill-defined at the plasma edge for divertor cases, thus q_{95} is still being used. A new global parameter, w_{07}, related to the radial width of the plasma shape at 70% of the maximum height is introduced to take into account the squareness present in most plasma shapes, in particular single-null diverted ones. We also provide a simple formula for the trapped fraction which includes the effects of triangularity. The trapped fraction is required for evaluating the neoclassical conductivity and bootstrap current in particular.

1. Introduction

The first steps to finding new plasma geometries and profiles, relevant for some specific objectives, consist of 0D analyses often performed with system codes like [3–6] and refs. therein. The first basic parameters are related to the plasma geometries, like volume and surfaces, which need to be characterized by a few number of parameters like major radius, minor radius and triangularity. The design of a new tokamak, for example, also consists of equilibrium and stability calculations based on a series of characteristic shapes and profiles. The equilibrium code CHEASE [7] can use the following simple shape definition for the plasma boundary:

$$R = R_0 + a\cos(\theta + \delta\sin\theta - \xi\sin 2\theta), \tag{1}$$

$$Z = \kappa a\sin(\theta + \xi\sin 2\theta), \tag{2}$$

where R_0, a, κ, δ and ξ are the plasma major radius, minor radius, elongation, triangularity and related to the plasma squareness respectively. We use the following definitions:

E-mail address: Olivier.Sauter@epfl.ch

http://dx.doi.org/10.1016/j.fusengdes.2016.04.033
0920-3796/

$$
\begin{aligned}
R_0 &= R_{geom} = \frac{R_{\max} + R_{\min}}{2},\\
a &= r_{edge} = \frac{R_{\max} - R_{\min}}{2},\\
\epsilon &= \frac{a}{R_0},\\
\kappa &= \kappa_{edge} = \frac{Z_{\max} - Z_{\min}}{R_{\max} - R_{\min}},\\
\delta &= \delta_{edge} = \frac{\delta_{top} + \delta_{bottom}}{2},\\
\delta_{top} &= \frac{R_0 - R(Z = Z_{\max})}{a},\\
\delta_{bottom} &= \frac{R_0 - R(Z = Z_{\min})}{a}.
\end{aligned}
\tag{3}
$$

They are defined for any given flux surface including the last closed flux surface (LCFS) and including non up-down symmetric and diverted shapes. They are evaluated at the plasma edge, if not indicated otherwise, as for example in Eq. (3). The aim is to obtain the basic global plasma shape characteristics based on these parameters. The "previous" formulas tested in this paper and eventually modified are the following [8,9]:

$$
I_p^{prev} = \frac{5a^2 B_0}{q_{95} R_0}\left[\frac{1+\kappa_{95}^2(1+2\delta_{95}^2-1.2\delta_{95}^3)}{2}\right]\left[\frac{1.17-0.65\epsilon}{(1-\epsilon^2)^2}\right], \tag{4}
$$

$$
V^{prev} = 2\pi^2 R_0 a^2 \kappa_{95}, \tag{5}
$$

$$
B_p^{prev} = \frac{I_p}{5af(\kappa_{95})}, \tag{6}
$$

$$
A_p^{prev} = 2\pi R_0 (2\pi a f(\kappa_{95})) = 4\pi^2 R_0 a f(\kappa_{95}), \tag{7}
$$

$$
f(\kappa_{95}) = \sqrt{\frac{1+\kappa_{95}^2}{2}}. \tag{8}
$$

These relations, or variants of these, have been used for the ITER design since the end of the eighties ([8,9] and refs. therein) and are used in present system codes for DEMO studies for example [4–6]. Other more "recent" formulas, in particular for the volume, have been determined including the edge shaping parameters and will be discussed as well [3,5] (using the up-down symmetric formulas from Ref. [5] in some cases):

$$
V^{rec} = 2\pi^2 R_0 a^2 \kappa \left[1 - (1 - \frac{8}{3\pi})\delta\epsilon\right], \tag{9}
$$

$$
A_p^{rec} = 4\pi^2 R_0 a f(\kappa) = 4\pi^2 R_0 a \sqrt{(1+\kappa^2)/2}, \tag{10}
$$

$$
L_p^{rec} = 4\kappa E(m = 1 - 1/\kappa^2), \tag{11}
$$

$$
S_\phi^{rec} = \pi a^2 \kappa, \tag{12}
$$

where $E(m)$ is the complete elliptic integral of the second kind and Eq. (11) is the exact formula for the perimeter of an ellipse of elongation κ (see also Appendix A).

2. Equilibria and method used

The equilibria used in this paper are shown in Fig. 1, normalized to their geometric major radius (a) or not (b). These equilibria have been calculated with the CHEASE fixed boundary equilibrium code [7] with various q profiles and edge κ, δ values. The values labelled "$_{95}$" are values at $\psi_{\rm norm} = 95\%$, that is at a given flux surface slightly inside the LCFS, where ψ is the poloidal flux with the general definition given in [12]. This was first used to define an equivalent edge safety factor for diverted plasmas, since $q_{\rm edge}$ becomes infinite in this case. The value of q_{95} does represent a useful parameter, for example when near or below 2 it is usually ideal MHD unstable. It happens that values defined in Eq. (3) have also been defined at $\psi_{\rm norm} = 95\%$, yielding κ_{95} and δ_{95}, for example for the volume of the LCFS as in Eq. (5). This is not necessary since the plasma shape is well defined up to the last closed flux surface and is actually misleading since they do not represent adequately the shape at $\psi_{\rm norm} = 100\%$ as will be seen below, but represent the shape at $\psi_{\rm norm} = 95\%$.

The values and formulas which will be discussed in this paper are related to the volume inside the LCFS, V, the surface area around the LCFS in the toroidal and poloidal direction, named A_p, the surface of the plasma cross-section in the radial and poloidal direction, named S_ϕ, the poloidal length around the plasma cross-section L_p and the plasma current I_p, yielding the average poloidal magnetic field B_p:

$$
V = \int dV = 2\pi \int \frac{R}{|\nabla\psi|} dl_p d\psi, \tag{13}
$$

$$
A_p = 2\pi \int R dl_p, \tag{14}
$$

$$
S_\phi = \int d\sigma_\phi = \int \frac{1}{|\nabla\psi|} dl_p d\psi, \tag{15}
$$

$$
L_p = \int dl_p, \tag{16}
$$

$$
I_p = \int j_\phi d\sigma_\phi, \tag{17}
$$

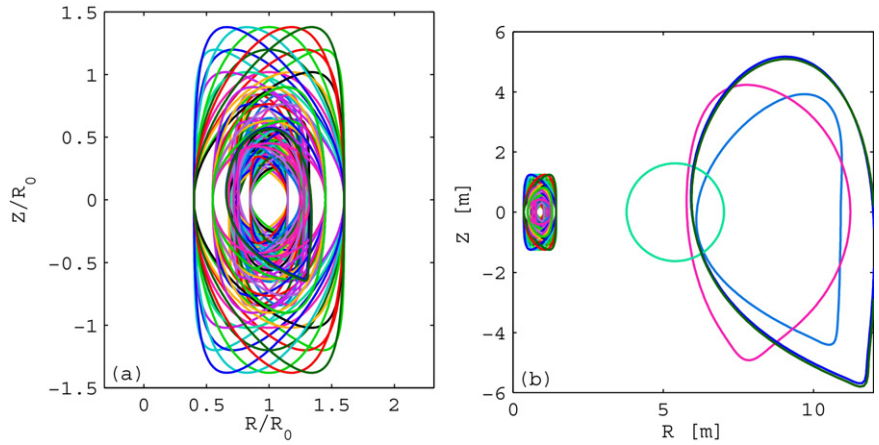

Fig. 1. Plasma boundaries used to compute the various quantities with the CHEASE equilibrium code. (a) Shapes normalized to R_0, (b) shapes in [m]. 16 out of 99 equilibria are not up-down symmetric.

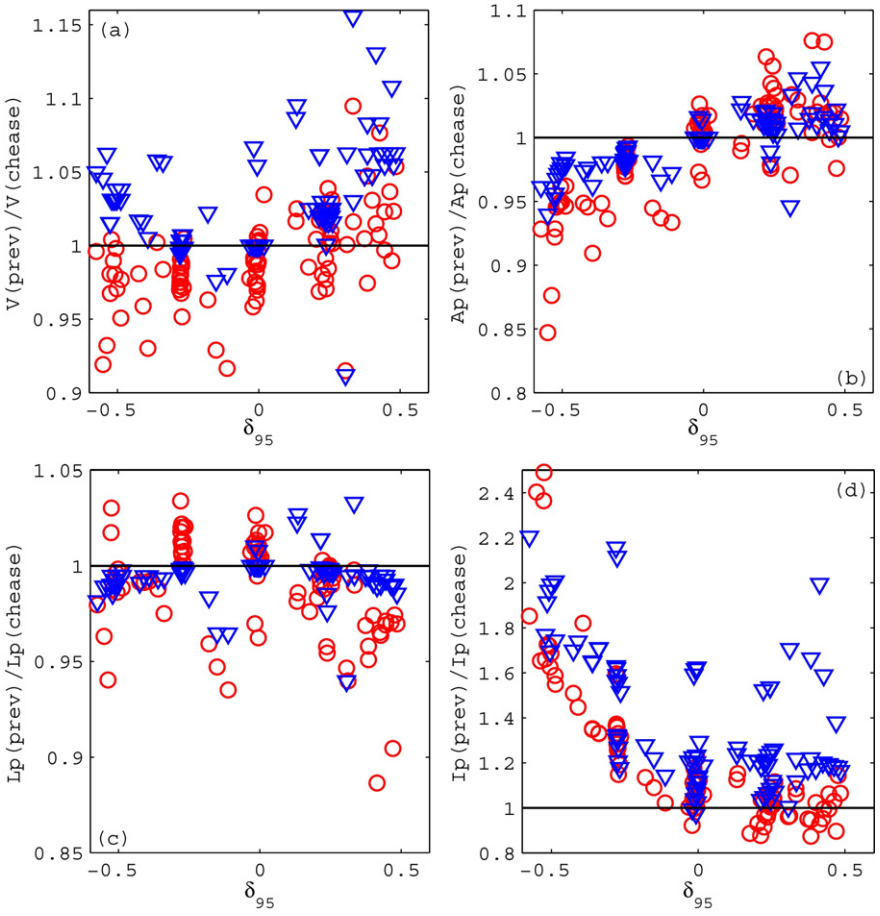

Fig. 2. Previous formulas to be tested divided by the respective values obtained with the CHEASE code for: (a) Volume Eq. (5) (circles) and Eq. (9) (triangles), (b) Area A_p Eq. (7) (circles) and Eq. (10) (triangles), (c) poloidal length Eq. (20) (circles) and Eq. (11) (triangles), and (d) Plasma current Eq. (4) (circles) and Eqs. (11) and (12) of Ref. [3] (triangles). (For interpretation of the references to color in text, the reader is referred to the web version of the article.)

$$B_p = \frac{\int B_p dl_p}{\int dl_p} = \frac{\mu_0 I_p}{L_p}, \tag{18}$$

From Eqs. (6), (16) and (18) we can write the previous formula used for L_p:

$$B_p = \frac{\mu_0 I_p}{L_p} = \frac{4\pi 10^{-7} I_p}{2\pi \tilde{L}_p} = \frac{I_p[MA]}{5\tilde{L}_p}, \tag{19}$$

$$L_p^{prev} = 2\pi \tilde{L}_p^{prev}, \tag{20}$$

$$\tilde{L}_p^{prev} = af(\kappa_{95}). \tag{21}$$

We can now plot the previous formulas divided by the exact values obtained by CHEASE versus δ_{95} for example. Eqs. (5), (7), (20) and (4) are shown in Fig. 2 (red circles). We see that the volume is within 4% in the positive δ range but clearly deviates at negative triangularity and large positive δ. We also see a wide spread, not centered around 1, of the fit at zero triangularity. This is because κ_{95} and not κ is used in Eq. (5) which under-predicts slightly the volume as discussed below. The flux surface area also deviates mainly for negative δ. On the other hand the value of L_p is not very accurate for both positive and negative triangularities. Finally the most striking problem is with the plasma current, which is over-estimated by a factor of up to two at triangularities near −0.6. The formula for I_p^{prev} does depend on triangularity, Eq. (4), however it has been constructed for positive δ plasma boundaries and therefore does not follow the correct trend at negative δ. In more recent works, the value of the edge shaping parameters has been used and we show Eqs. (9), (10) and (11) in Fig. 2 as well with blue triangles, and I_p from Eqs. (11) and (12) of Ref. [3]. Note that even if $\delta\epsilon$ is taken into account in the volume, for example, the overall more recent formulas do not fit the data much better. Even Eq. (11), which is exact for an ellipse and thus yields a ratio=1 for $\delta = 0$, tends to overestimate the CHEASE value for non up-down symmetric plasmas and $\delta \neq 0$ (Fig. 2(c), triangles).

3. Why using δ, κ rather than δ_{95}, κ_{95}?

In the new formulas, we shall use δ and κ even for I_p. Before presenting the new formulas, let us see the main dependencies of the terms considered and demonstrate why it is a better choice. First, the volume of an ellipse is exactly given by Eq. (5) with κ_{95} replaced by κ, and the volume, areas and length of a given flux surface are naturally best parametrized by the values of a, R_0, δ and κ of the respective flux surface, that is of the LCFS in particular. Let us look at the ratio A_p/L_p using Eqs. (7) and (20):

$$\frac{A_p^{prev}}{L_p^{prev}} = 2\pi R_0. \tag{22}$$

Thus we should have $A_p/(2\pi R_0 L_p) = 1$. This ratio is plotted in Fig. 3 versus $(\delta\epsilon)$ (stars) and versus $(\delta_{95}\epsilon)$ (open circles). First we see that it is not equal to 1, except for $\delta = 0$. Then we observe a nice alignment of the points using δ, while it is not at all the case with δ_{95}. The latter is due to the fact that the "penetration" of edge triangularity and elongation inside the LCFS depend on the q profile and the edge δ in particular. We show in Fig. 4 the various q profiles used in this set of equilibria, which are relatively standard with varying q_{95}

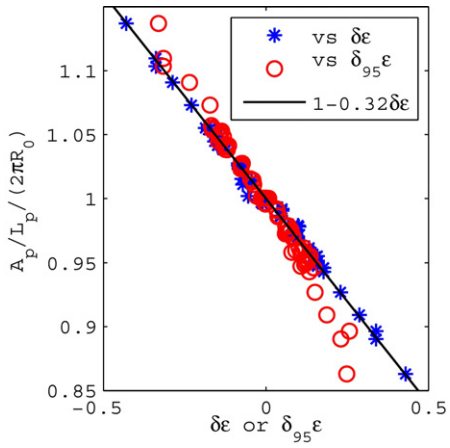

Fig. 3. $A_p/(2\pi R_0 L_p)$ from CHEASE versus $(\delta\epsilon)$ in blue stars and $(\delta_{95}\epsilon)$ in red open circles. In black, the line $y = 1 - 0.32x$ is plotted. (For interpretation of the references to color in this figure legend, the reader is referred to the web version of the article.)

values, and the related $l_i(3)$ [7] values, which are standard as well. Note that l_i values between 0.5 and 1.1 are expected in most scenarios. Positive and negative δ lead to very different "penetration" of the shaping parameters and thus very different δ and κ profiles as seen in Fig. D24. Note that the ratio of κ/κ_{95} tend to increase with κ and δ and is within 10% in this set of equilibria, except at very high δ where it reaches 20%. A difference of 10% in estimated volume would directly reflect in a different expected fusion power and therefore can be important in DEMO studies. On the other hand, even if using the new formulas, an attractive solution found by a 0D system code should be checked with an equilibrium solver and 1D studies. Note that the ratio of δ/δ_{95} is between 0.9 and 1.4 in the equilibria used here.

4. New formulas

We can now determine the new formulas. Following the observed relation between A_p and L_p (Eq. (22)) and Fig. 3 (solid line) we first define:

$$A_p^{new} = 2\pi R_0(1 - 0.32\delta\epsilon)L_p^{new}. \tag{23}$$

We then need to find L_p^{new}. Using Eq. (20) we start from $L_p \sim 2\pi a f(\kappa)$ and we plot $L_p/(2\pi a)$ versus elongation in Fig. 5. We see that actually it is relatively linear in the usual range of elongations [1, 2.5]. Actually the function $f(\kappa)$ can be fitted with a line within 1.5% for $0.8 < \kappa < 3.1$ (see Appendix A). Fig. 5 shows that $0.45 + 0.55\kappa$ is simpler and more appropriate, thus defining the new $f^{new}(\kappa)$ function to be used (Eq. (A.2)). There remains a small dependence on triangularity as seen in Fig. 5(c), leading to less than 2% deviations. Using the more precise formula from Ramajunan for $f(\kappa)$ [13], Eq. (A.1), which yields the exact perimeter for a pure ellipse (Appendix A), reduces the scatter as seen in Fig. 5(d). However for shapes with some squareness or up-down asymmetric shapes, it does not reduce the error significantly.

Let us first discuss the effect of up-down asymmetry. In this study, there are 16 equilibria out of 99 with single-null up or down, based on typical present tokamak equilibria with positive δ cases, thus as well ITER- and DEMO-like, and based on Ref. [2] and TCV experiments for negative δ. We have also used the series of TCV experiments used to study the effect on rotation of changing the X-point major radius position from HFS to LFS [10,11] (where HFS and LFS are the high- and low-field sides respectively). In all these cases we find that taking the average κ, δ values between the top and bottom parts, as defined in Eq. (3) and w_{07} in Eq. (24), resolves the main differences with respect to up-down symmetric plasmas. This is expected since all the geometric quantities discussed here are the sum of the bottom and top parts (with respect to $Z = Z_{axis}$). This is of course also why we use formulas of the form $V[\delta] = V_0(1 + a\delta + b\delta^2)$ which yields $V_{top} + V_{bot} = V[\delta = (\delta_{top} + \delta_{bot})/2] + V_0 b(\delta_{top} - \delta_{bot})^2/4$, thus only an error of less than 2% even if $|\delta_{top} - \delta_{bot}| = 0.3$, for $b \le 1$. The main outliers in Fig. 5 are actually those with significant squareness, like the ones in Refs. [10,11] and those with $\xi \neq 0$ in Eqs. (1) and (2) as discussed below.

The effect of squareness is illustrated in Fig. 6, where three shapes with $\kappa = 1.7$, $\delta = 0.4$ and $\xi = 0.2$, 0 and -0.3 are shown (Eqs. (1) and (2)). It is clear that these shapes have different perimeter, surfaces and volume, although they have the same elongation, triangularity and aspect ratio. Actually the yellow line reaching 1.06 in Fig. 5(c and d) and the light blue line reaching 0.97, at $\delta = 0.4$, correspond to the equilibria with $\xi = 0.2$ and -0.3 shown in Fig. 6, respectively. We propose to take the radial distance between the points at 70% of the maximum height as a measure of the plasma squareness. From Eqs. (1) and (2) and $\xi = 0$, we see that it corresponds to the points at $\theta = \arcsin(0.7) \sim \pm 45^\circ$ and $\pm 135^\circ$. The distance w_{07} is normalized by the value obtained with $\xi = 0$:

$$w_{07}^{top} = \frac{R_{LFS}[Z = Z_0 + 0.7(Z_{\max} - Z_0)] - R_{HFS}[Z = Z_0 + 0.7(Z_{\max} - Z_0)]}{2a\cos[\arcsin(0.7)]},$$

$$w_{07}^{bot} = \frac{R_{LFS}[Z = Z_0 + 0.7(Z_{\min} - Z_0)] - R_{HFS}[Z = Z_0 + 0.7(Z_{\min} - Z_0)]}{2a\cos[\arcsin(0.7)]},$$

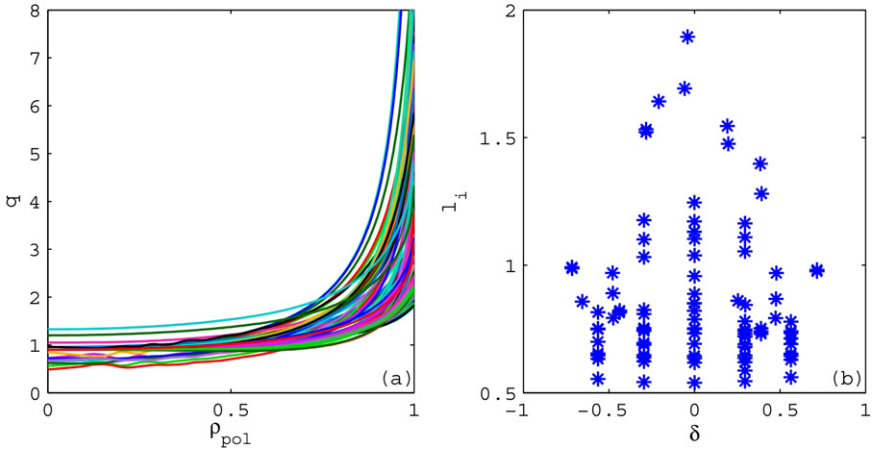

Fig. 4. (a) Various q profiles from the set of equilibria shown in Fig. 1. (b) Internal inductance $l_i(3)$ [7] versus δ for these equilibria.

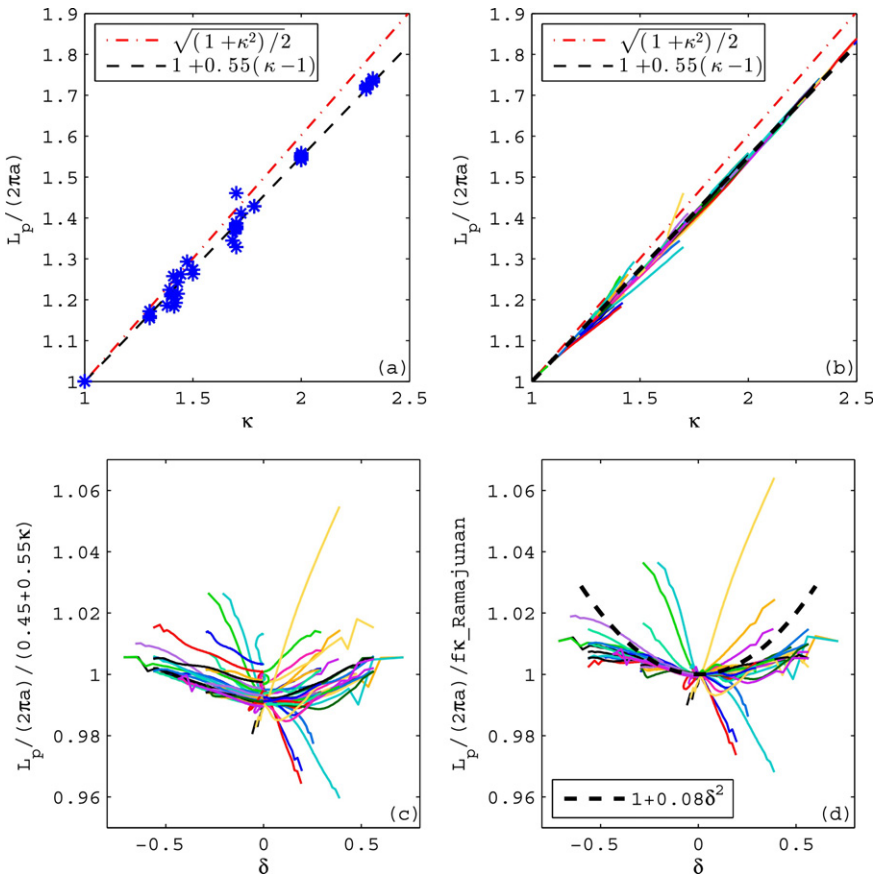

Fig. 5. Dependence of $L_p^{chease}/(2\pi a)$ versus κ. (a) LCFS values, (b) profiles for each equilibrium using local flux surface values. Dashed-dotted lines correspond to $f(\kappa) = \sqrt{(1+\kappa^2)/2}$ and dashed lines to $1+0.55(\kappa-1)$. (c) Profiles from each equilibrium of $L_p^{chease}/(2\pi a)/(1+0.55(\kappa-1))$ versus δ. (d) Same as (c) but using $f(\kappa)^{Ramanujan}$, Eq. (A.1), yielding the perimeter of an ellipse as $2\pi a f(\kappa)$ [13], better for a pure ellipse but the linear fit proposed with $f = 0.45 + 0.55\kappa$ is accurate within 1% and is sufficient (see also Appendix A). (For interpretation of the references to color in text, the reader is referred to the web version of the article.)

and averaged:

$$w_{07} = \frac{w_{07}^{top} + w_{07}^{bot}}{2}. \tag{24}$$

In this way, w_{07} is near 1 for small squareness and $(w_{07}-1)$ yields the degree of squareness. There is a small δ dependence that we could have added into the definition, using Eqs. (1) and (2) (see Appendix C), but this will be included in the resulting formulas in any case. The relation between ξ and w_{07} for plasma shapes provided by Eqs. (1) and (2) is discussed in Appendix C. We plot now the value of L_p divided by $2\pi a[1+0.55(\kappa-1)](1+0.08\delta^2)$ versus w_{07} in Fig. 7. We see that there remains a relatively linear dependence on w_{07} which we can add to the final formula. This leads to the following formulas for L_p^{new} and thus A_p^{new} from Eq. (23):

$$L_p^{new} = 2\pi a[1+0.55(\kappa-1)](1+0.08\delta^2)[1+0.2(w_{07}-1)], \tag{25}$$

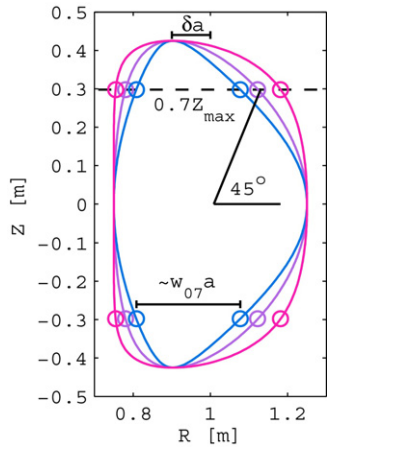

Fig. 6. Shapes with R values at $Z = 0.7(Z_{min/max} - Z_{axis})$. The distance marked "$\sim w_{07}a$" is $w_{07}(2a\cos[\arcsin(0.7)])$ and $w_{07}\sim 1$ in case of an up-down symmetric shape with $\xi = 0$ as defined in Eqs. (1) and (2). Note that w_{07} is the average between the top and bottom values for up-down asymmetric plasmas.

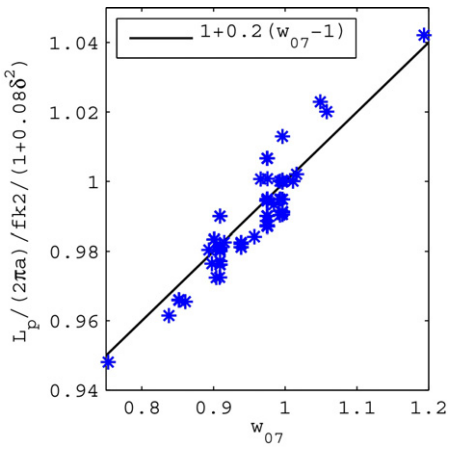

Fig. 7. $L_p^{chease}/\{2\pi a[1+0.55(\kappa-1)](1+0.08\delta^2)\}$ versus w_{07}.

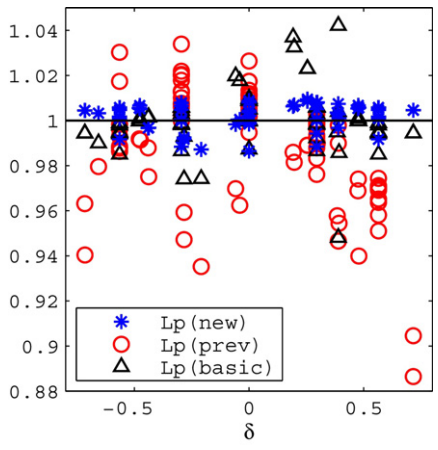

Fig. 8. L_p/L_p^{chease} versus δ for L_p^{new} Eq. (25)), L_p^{prev} Eq. (20) and L_p^{basic} Eq. (27).

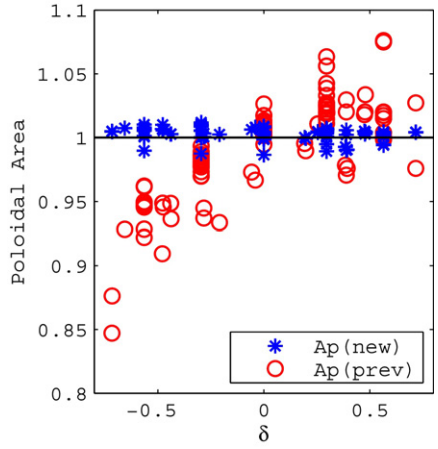

Fig. 9. (a) A_p^{new}/A_p^{chease} (Eq. (26)) and A_p^{prev}/A_p^{chease} (Eq. (7)) versus triangularity.

$$A_p^{new} = 2\pi R_0(1 - 0.32\delta\epsilon)L_p^{new}. \tag{26}$$

Fig. 8 shows the comparison with the CHEASE results of the new formula for L_p^{new} (stars) versus δ, yielding less than a 2% error, as compared to the previous formula having up to 12% errors (Eq. (20)). We also show the basic straightforward relation:

$$L_p^{basic} = 2\pi a[1 + 0.55(\kappa - 1)], \tag{27}$$

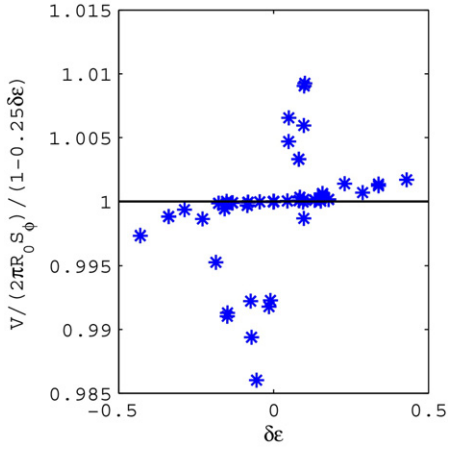

Fig. 11. $V^{chease}/(2\pi R_0 S_\phi)/(1 - 0.25\delta\epsilon)$ vs $\delta\epsilon$.

in Fig. 8 with triangles leading to a 5–6% error (same overall accuracy with Ramanujan's formula). Note that the $(1 + 0.08\delta^2)$ dependence is illustrated in Fig. 5(d) and appears a bit too strong. However, once the dependence on w_{07} is taken into account, the resulting term does follow this δ dependence. This is because there is a small δ dependence in w_{07} as mentioned earlier and can be verified by the fact that there remains no significant δ dependence in Fig. 8 (stars). In Fig. 9, we show the comparison for A_p, comparing Eqs. (26) (stars) and (7) (circles) with the CHEASE results. The new formulas for L_p and A_p are better and accurate within 2%.

Let us now look at the volume (Eq. (13)) and poloidal cross-section surface S_ϕ (Eq. (15)). Again from the formulas valid for an ellipse, we expect $V = 2\pi^2 a^2 R_0 \kappa$ and $S_\phi = \pi a^2 \kappa$, thus $V/S_\phi = 2\pi R_0$. We plot in Fig. 10 the value from CHEASE of $V/(2\pi R_0 S_\phi)$ versus $\delta\epsilon$, for both the edge values (a) and the profiles for each equilibrium using the local values (b). We see that it is not equal to one, except for zero triangularity, and follows well a linear dependence versus $(\delta\epsilon)$, as seen previously for A_p/L_p. We also show the dashed line corresponding to Eq. (9) with $1 - 8/3\pi \approx 0.15$ yielding a slightly different dependence on $\delta\epsilon$. Fig. 11 shows that the following fit provides the volume from the cross-section within less than 2%, even for the special outlier shapes:

$$V^{new} = 2\pi R_0(1 - 0.25\delta\epsilon)S_\phi^{new}. \tag{28}$$

Looking now at the surface $S_\phi/(\pi a^2 \kappa)$, we find that it is also essentially linear with w_{07} as seen in Fig. 12, for both the edge

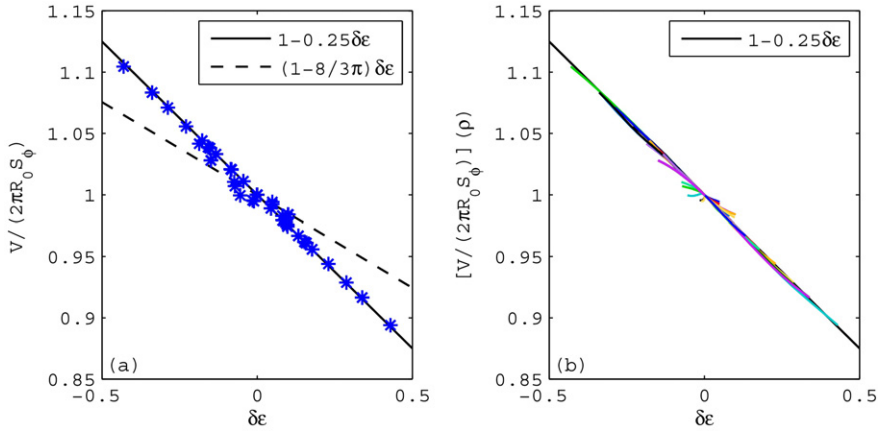

Fig. 10. $V^{chease}/(2\pi R_0 S_\phi)$ vs $\delta\epsilon$ for the equilibria considered ((a) edge values, (b) profiles for each equilibria). Again, there remains a relatively strong dependence on both δ and ϵ, different from $(1 - 8/3\pi)$ used previously.

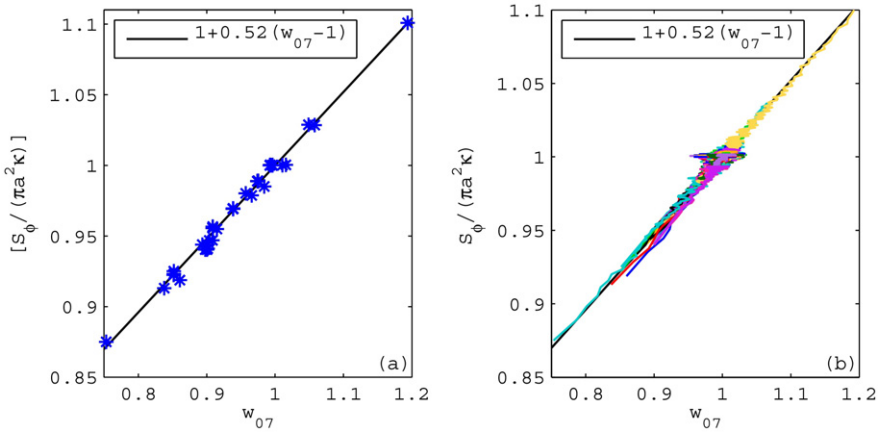

Fig. 12. $S_\phi^{chease}/(\pi a^2\kappa)$ vs w_{07} for the equilibria considered ((a) edge values, (b) profiles for each equilibria).

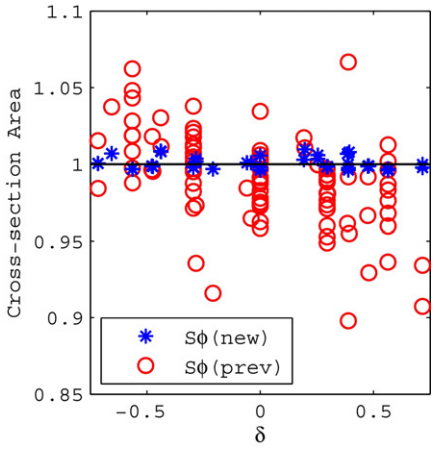

Fig. 13. (a) $S_\phi^{new}/S_\phi^{chease}$ (Eq. (29)) and $S_\phi^{prev}/S_\phi^{chease}$ (with $S_\phi^{prev}=\pi a^2\kappa_{95}$) versus triangularity. Note that using $\pi a^2\kappa$ leads to values mainly between 1 and 1.15, so not better on average than $\pi a^2\kappa_{95}$ since it is over-estimating the cross-section area for $\delta \neq 0$ or $w_{07} \neq 1$ (similarly for the volume as seen in Fig. 2(a)).

values (a) and the profiles (b). We can therefore define the new formula for the surface S_ϕ as follows:

$$S_\phi^{new} = \pi a^2\kappa[1 + 0.52(w_{07} - 1)], \tag{29}$$

with w_{07} defined by Eq. (24) as before. The ratio with the CHEASE values is shown in Fig. 13 versus δ and compared to the previous formula taken from $S_\phi^{prev}=V^{prev}/(2\pi R_0)=\pi a^2\kappa_{95}$ (Eq. (5)). We see that Eq. (29) is quite accurate and we get the same for the volume (Fig. 14), new fits within 2% of the CHEASE results. Note that the previous formulas did not take into account the effect of squareness. As mentioned above, more recent formulas do take into account the effects of $\delta\epsilon$, as well as using the local values instead of the values at $\psi_{norm} = 95\%$. However the present new formulas are shown to be more accurate also for positive δ. Looking closer at the formulas for A_p and L_p in Ref. [5], first we note that $E_1(\kappa) = 2/\pi\,\kappa E(\sqrt{1-1/\kappa^2})$ can be approximated by $0.55\kappa + 0.45$ as demonstrated above, which means that L_p^{basic}, Eq. (27), is actually the same as Eq. (13) of Ref. [5] since $\Theta_L^* \approx 1$ with the above approximation. Similarly, one can show that $\arcsin(\sqrt{1-1/\kappa^2})/\sqrt{1-1/\kappa^2}$ can be approximated by $\kappa/(0.65\kappa + 0.35)$ which yields $A_p/L_p/(2\pi R_0)|^{ref5} \approx 1 - 0.19\,\delta\epsilon$, almost independent of κ for $\kappa > 1.4$. It confirms that the main dependence is on $\delta\epsilon$ although with a different coefficient from the value 0.32 found in Fig. 3.

We can now look at the formula for the plasma current or equivalently for q_{95}. From the cylindrical definition, we have $q_{cyl} = 2\pi aB_0/2\pi R_0 B_p = aL_pB_0/R_0\mu_0 I_p$. One has also used $q_{eng} = 5B_0a^2\kappa/R_0Ip$ as characteristic safety factor, identical to q_{cyl} taking $L_p = 2\pi a\kappa$ and which has similarities with Eq. (4). Starting from these considerations, we obtain the following formula for q_{95} and I_p[MA]:

$$q_{95}^{new} = \frac{4.1a^2B_0}{R_0 I_{p,MA}}[1 + 1.2(\kappa - 1) + 0.56(\kappa - 1)^2]$$

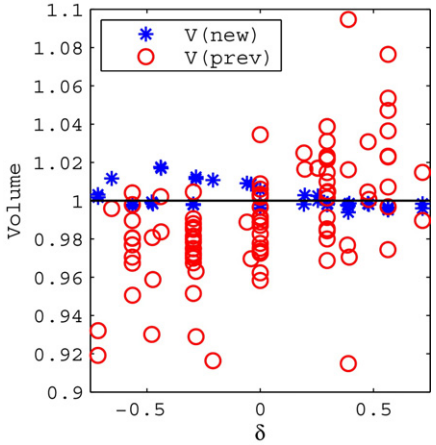

Fig. 14. (a) V^{new}/V^{chease} (Eq. (28)) and V^{prev}/V^{chease} (Eq. (5)) versus triangularity.

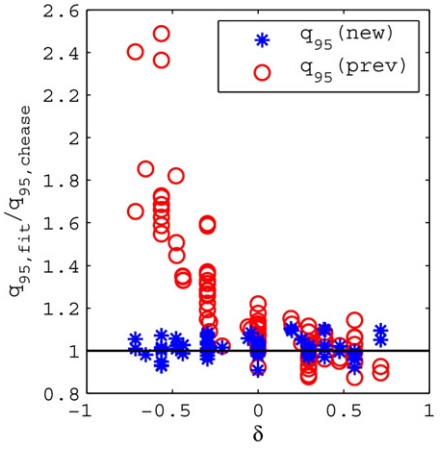

Fig. 15. (a) $q_{95}^{new}/q_{95}^{chease}$ versus δ, using I_p from the respective CHEASE equilibrium.

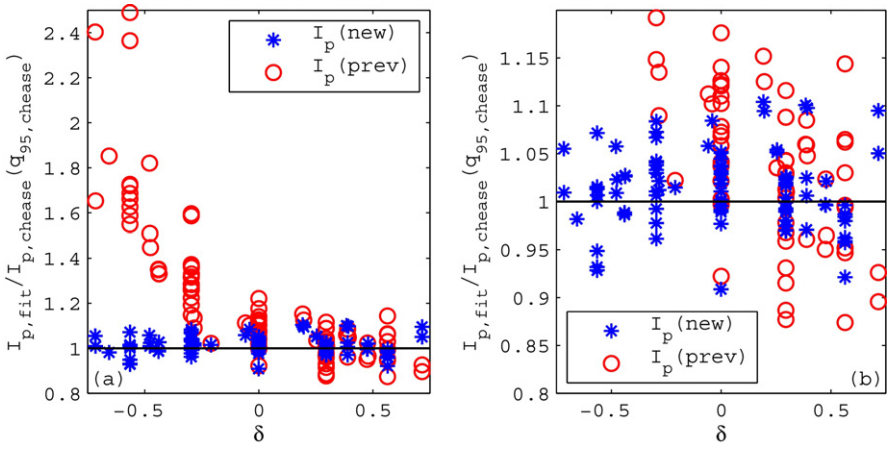

Fig. 16. (a) I_p^{new}/I_p^{chease} versus δ, using q_{95} from the respective CHEASE equilibrium. (b) Zoom of the y-axis close to 1.

$$\times (1+0.09\delta+0.16\delta^2)\frac{1+0.45\delta\epsilon}{1-0.74\epsilon}[1+0.55(w_{07}-1)], \tag{30}$$

$$I_{p,MA}^{new} = \frac{4.1a^2B_0}{R_0 q_{95}}[1+1.2(\kappa-1)+0.56(\kappa-1)^2] \times (1+0.09\delta+0.16\delta^2)\frac{1+0.45\delta\epsilon}{1-0.74\epsilon}[1+0.55(w_{07}-1)]. \tag{31}$$

The ratio of q_{95} over the CHEASE values are shown in Fig. 15 and similarly for the plasma current in Fig. 16. It shows that Eqs. (30) and (31) are accurate within 10% for the cases considered here over the whole range of triangularities, including in particular negative δ. The fit has been constructed such that the dependence of each term is recovered individually. This is shown in Appendix B, Fig. B21. For example, using Eq. (30) without the κ term, shows a dependence versus κ of $(1+1.2(\kappa-1)+0.56(\kappa-1)^2)$ (Fig. B21(a)). This allows to naturally take into account non up-down symmetric plasmas, as discussed earlier, and ensure realistic dependencies. We have tried to minimize coupled parameters and have checked that it does not lead to more accurate formulas.

For completeness, we verify the last formula for the average B_p, by comparing the result using the new formulas for I_p (Eq. (31)) and L_p (Eq. (25)) introduced into Eq. (19) with the direct result from CHEASE: $B_p^{chease} = \mu_0 I_{p,MA}^{chease}/L_p^{chease}$. We see that they follow one another within 10% over a large range.

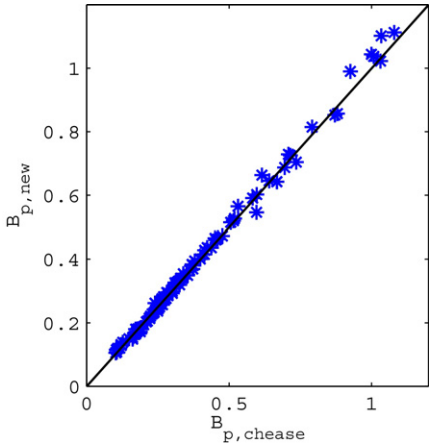

Fig. 17. B_p^{new} versus B_p^{chease} using the CHEASE q_{95} value of the respective equilibria and the formulas for I_p^{new} and L_p^{new}, Eqs. (31) and (25), to calculate $B_p^{new} = \mu_0 I_{p,MA}^{new}/L_p^{new}$.

***Fig. 17

5. Trapped fraction

The trapped fraction f_t is defined by:

$$f_t = 1 - \frac{3}{4}\langle B^2\rangle \int_0^{1/B_{\max}} \frac{\lambda d\lambda}{\langle\sqrt{1-\lambda B}\rangle}, \tag{32}$$

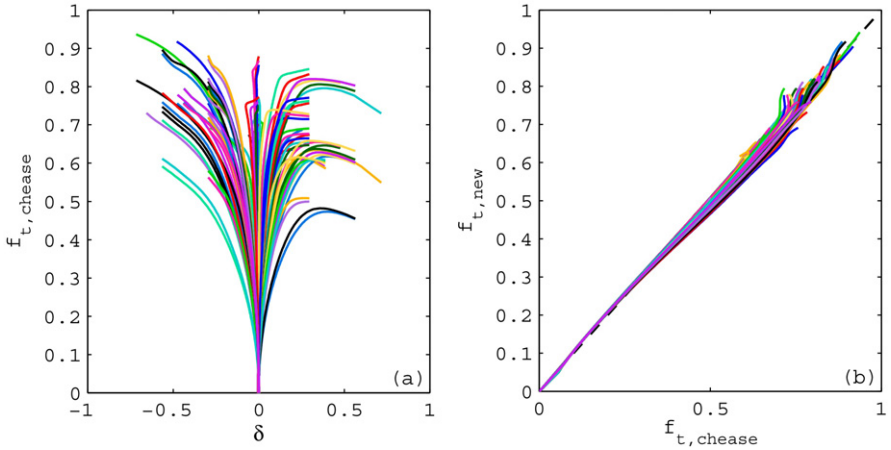

Fig. 18. (a) Trapped fraction profiles from CHEASE for the various equilibria versus δ. (b) Trapped fraction from Eq. (34), using the local values, versus the CHEASE calculation.

where $\langle\cdot\rangle$ means the flux surface average. It is known to be important for the calculation of the bootstrap current density [14], however it is the generic cause of neoclassical effects. In particular it is important for the plasma conductivity, therefore loop voltage and flux consumption. In this respect, let us note that it is good to include the bootstrap current formulas [14] inside the system codes, since fusion reactors will require a high bootstrap fraction. It is even more important to include the neoclassical conductivity as given by the similar formulas and to use the improved Spitzer conductivity, also given as simple fits of accurate simulations in [14]. These formulas require the trapped fraction, which can be difficult to calculate. We have recently extended a formula first given in [15] to include the effect of triangularity [16]:

$$\epsilon_{eff} = 0.67(1 - 1.4\delta|\delta|)\epsilon, \tag{33}$$

$$f_t = 1 - \frac{1-\epsilon_{eff}}{1+2\sqrt{\epsilon_{eff}}}\sqrt{\frac{1-\epsilon}{1+\epsilon}}, \tag{34}$$

$$f_t = \min(1, f_t(\text{Eq. (34)})). \tag{35}$$

The trapped fraction profiles for the equilibria studied in this paper are shown in Fig. 18(a) versus triangularity. In Fig. 18(b) we show the new formula, Eq. (34), versus the CHEASE f_t profiles. They follow one another within 10% over a wide range, with cases almost up to 1. It can even be used for 3D geometries with appropriate local parameters and with not too pronounced 3D equilibrium effects [17].

6. Conclusion

New formulas have been derived for the main geometric quantities, including the trapped fraction, as well as the relation between plasma current and safety factor, to be used for example in 0D system codes [1,2]. These formulas are valid over a wide range of parameters, in particular at negative triangularity and various aspect ratio. Even at standard triangularity and q_{95} values, the new formulas are more accurate. They remove in particular the systematic error introduced by using the geometric parameters like κ and δ at the $\psi_{norm} = 95\%$ flux surface. Edge values are now used to describe the last closed flux surface, being diverted or limited, up-down symmetric or not. Recent formulas were using appropriate edge parameters, however we have shown that the clear main dependence of A_p/L_p and V/S_ϕ on $(\delta\epsilon)$ is better taken into account in the new formulas. Nevertheless even the cross-section area is not sufficiently well represented by $S_\phi = \pi a^2\kappa$. A new parameter has been introduced, w_{07}, related to the distance along the major radius of the flux surface at 70% of the maximum height. This enables to take into account the squareness, for example, of the flux surface which is present in diverted geometries as well, in particular near the X-point. The new formulas are detailed in this paper and summarized here for convenience:

$$\begin{aligned}
L_p^{new} &= 2\pi a[1 + 0.55(\kappa - 1)](1 + 0.08\delta^2)[1 + 0.2(w_{07} - 1)],\\
A_p^{new} &= 2\pi R_0(1 - 0.32\delta\epsilon)L_p^{new},\\
V^{new} &= 2\pi R_0(1 - 0.25\delta\epsilon)S_\phi^{new},\\
S_\phi^{new} &= \pi a^2\kappa[1 + 0.52(w_{07} - 1)],\\
I_{p,MA}^{new} &= \frac{4.1a^2B_0}{R_0q_{95}}[1 + 1.2(\kappa - 1) + 0.56(\kappa - 1)^2](1 + 0.09\delta + 0.16\delta^2)\frac{1 + 0.45\delta\epsilon}{1 - 0.74\epsilon}[1 + 0.55(w_{07} - 1)],\\
q_{95}^{new} &= \frac{4.1a^2B_0}{R_0I_{p,MA}}[1 + 1.2(\kappa - 1) + 0.56(\kappa - 1)^2](1 + 0.09\delta + 0.16\delta^2)\frac{1 + 0.45\delta\epsilon}{1 - 0.74\epsilon}[1 + 0.55(w_{07} - 1)],\\
B_p^{new} &= \frac{I_p^{new}}{5(L_p^{new}/2\pi)},\\
f_t &= \min\left[1 - \frac{1-\epsilon_{eff}}{1+2\sqrt{\epsilon_{eff}}}\sqrt{\frac{1-\epsilon}{1+\epsilon}}; 1\right].
\end{aligned} \tag{36}$$

Acknowledgements

This work was supported in part by the Swiss National Science Foundation. The author would like to thank Drs. M. Kikuchi and D. Chen for useful discussions and for motivating these studies. Dr. S. Yu. Medvedev is thanked for providing DEMO-like equilibria.

Appendix A. Perimeter L_p

Accurate formulas for the perimeter of an ellipse have been developed by Ramanujan [13]. The less complicated, yet very accurate, formula is given by:

$$f(\kappa)^{Ramanujan} = 1.5(\kappa + 1) - 0.5\sqrt{(3\kappa + 1)(\kappa + 3)}. \tag{A.1}$$

We have noticed that this relation is almost linear with κ in the typical tokamak range. We compare the previous function $f(\kappa)$ (Eq. (8), with κ instead of κ_{95}) and the new proposed formula:

$$f(\kappa)^{new} = 1 + 0.55(\kappa - 1). \tag{A.2}$$

They are shown in Fig. 19 divided by Eq. (A.1) versus elongation. It shows that the new relation, Eq. (A.2), is accurate within 1.5% for

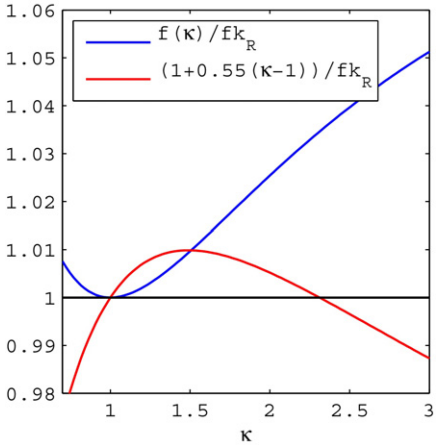

Fig. 19. Previous form of $f(\kappa) = \sqrt{(1+\kappa^2)/2}$, Eq. (8) and new form $f(\kappa)^{new} = 0.45 + 0.55\kappa$ divided by Ramanujan formula fk_R given in Eq. (A.1).

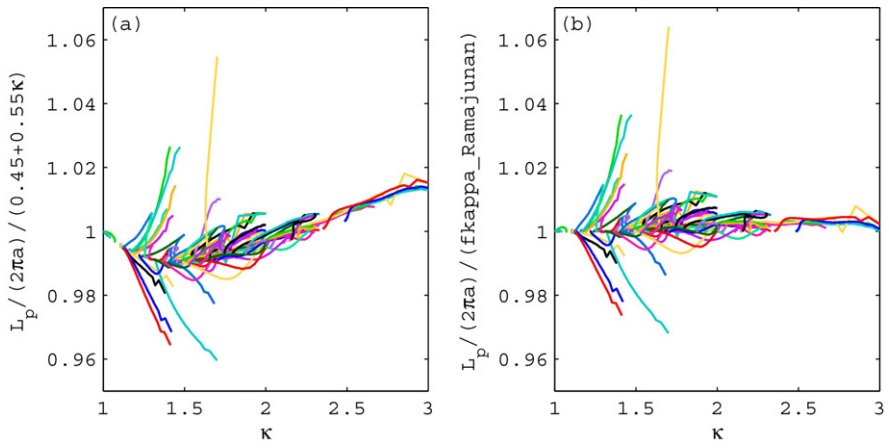

Fig. 20. Profiles for each equilibrium of $L_p/(2\pi a f(\kappa))$ with either (a) $f(\kappa)^{new}$, Eq. (A.2) or (b) $f(\kappa)^{Ramanujan}$, Eq. (A.1).

κ between 0.8 and 3.1. The previous form, Eq. (8), is less accurate. Note that $f(\kappa)$ is simply the approximation of $2/\pi\, E(m=1-1/\kappa^2)$ with $E(m)$ the complete elliptic integral of the second kind.

We can compare with the values of L_p obtained by CHEASE. Fig. 20(a) shows $L_p/(2\pi a f(\kappa)^{new})$ versus κ and (b) shows $L_p/(2\pi a f(\kappa)^{Ramanujan})$. The κ dependence is better extracted with Eq. (A.1), however the gain of 1–2% does not resolve the deviation due to the squareness or to up-down asymmetry, leading to errors of order 4–6%, as discussed in the main text.

Appendix B. Test of I_p, q_{95} formula

We test the formula for q_{95}, hence of I_p. For each term in Eq. (30), the fit without the relevant term is compared to the CHEASE values and shown versus its dependent variable in Fig. B21, including the relevant line. For example:

$$q_{95}^{new,\mathrm{no}\kappa} = \frac{4.1a^2B_0}{R_0 I_{p,MA}}(1+0.09\delta+0.16\delta^2)\frac{1+0.45\delta\epsilon}{1-0.74\epsilon} \times [1+0.55(w_{07}-1)], \tag{B.1}$$

is plotted versus κ, including the line $[1+1.2(\kappa-1)+0.56(\kappa-1)^2]$ (Fig. B21(a)). We see that the fits follow relatively well the data. Improvements would require the knowledge of the current density profile, using l_i for example. However the fit is already accurate within 10%. One should directly use a code like CHEASE [7] if a better accuracy is required, since it can calculate all the quantities very fast.

Appendix C. Relation between ξ and w_{07} using Eqs. (1) and (2)

Many codes actually use Eqs. (1) and (2) to define the plasma boundary. Thus one can obtain the value of w_{07} relatively easily. First we show in Fig. C22(a) the relation between w_{07} and ξ for shapes defined by Eqs. (1) and (2) and with $1<\kappa<3$, $-0.8<\delta<0.8$ and $-0.5<\xi<0.65$, the latter being the maximum limits for ξ. We see that the relation is not symmetric and saturates at small positive values of ξ because the shape is already very "square". We also see that there is no dependence on κ, as expected, and little dependence on δ. The solid line is obtained from the analytical formula presented here below. First we note from Eq. (2) that the angle θ_{LFS}^{07} at which $Z=0.7\,Z_{max}$ must satisfy:

$$\theta_{LFS}^{07} + \xi \sin 2\theta_{LFS}^{07} = \arcsin(0.7). \tag{C.1}$$

Assuming $\theta_{LFS}^{07} = \arcsin(0.7)+\alpha$ with α small (note that $\alpha=0$ for $\xi=0$) and taking the LFS solution, we obtain:

$$\theta_{LFS}^{07} \approx \arcsin(0.7) + \frac{1-\sqrt{1+8\xi^2}}{4\xi}. \tag{C.2}$$

We check this result in Fig. C22(b) where we plot the *sin*() of the left-hand side of Eq. (C.1), using Eq. (C.2), divided by 0.7, which should yield 1. We see that it is accurate within 1.5%. Using this solution we can evaluate w_{07} from Eqs. (1) and (24) and taking first $\delta=0$. We obtain:

$$w_{07}^{anal,\delta\sim 0} = \frac{\cos[\theta_{LFS}^{07} - \xi\sin(2\theta_{LFS}^{07})]}{\sqrt{0.51}}, \tag{C.3}$$

with θ_{LFS}^{07} given in Eq. (C.2). This is the solid line shown in Fig. C22(a) which follows very well the points for $\delta=0$ (stars) over essentially the whole range of ξ. The other points are obtained with $\delta=\pm 0.5$ and ± 0.8. Calculating again w_{07} from Eqs. (1) and (24) but taking $\xi=0$ this time, we obtain:

$$w_{07}^{anal}(\xi=0) \approx 1 - \frac{0.49}{2}\delta^2. \tag{C.4}$$

It yields a reduction with δ as seen from the points being below the solid line in Fig. C22(a). We thus obtain the following full analytical formula for w_{07} by multiplying Eqs (C.3) and (C.4):

$$w_{07}^{anal} = \frac{\cos[\theta_{LFS}^{07} - \xi\sin(2\theta_{LFS}^{07})]}{\sqrt{0.51}}\left[1-\frac{0.49}{2}\delta^2\right]. \tag{C.5}$$

We show again w_{07} versus ξ in Fig. C23(a) but zooming near $\xi=0$ and adding the analytical line with $\delta=\pm 0.5$ and ± 0.8. In Fig. C23(b) we show w_{07} versus triangularity for various values of ξ. We see that the analytical formula is very good except at high δ and high positive ξ.

Appendix D. Elongation and triangularity profiles

For completeness we show the κ and δ profiles of the various equilibria used in this study in Fig. D24. For a same edge κ value, the elongation on axis can be very different, in particular for negative versus positive δ cases.

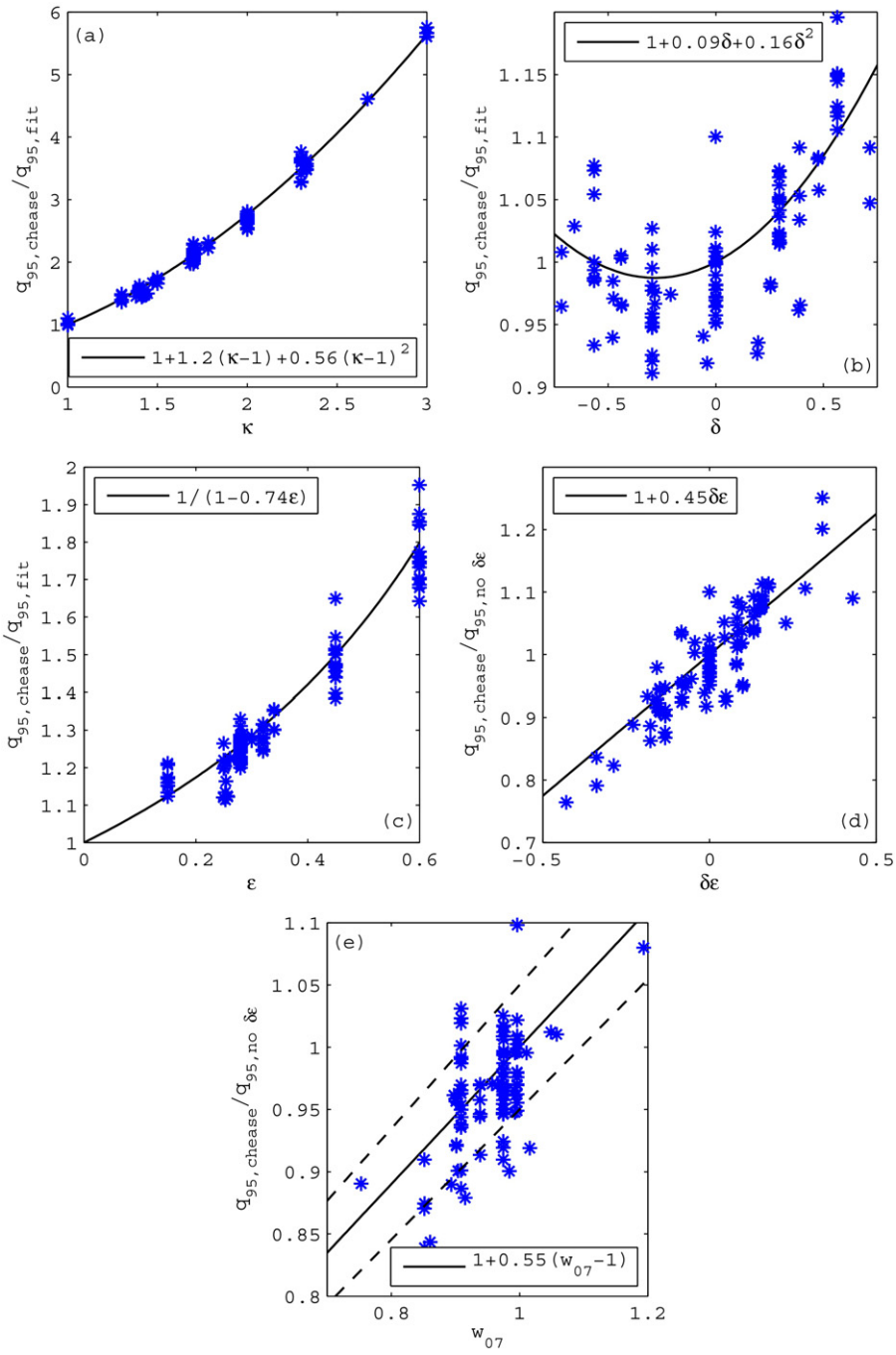

Fig. B21. $q_{95}^{chease}/q_{95}^{new,incomplete}$ with $q_{95}^{new,incomplete}$ from Eq. (30) without one of the term: (a) $q_{95}^{chease}/q_{95}^{new,no\,\kappa}$ versus κ. (b) $q_{95}^{chease}/q_{95}^{new,no\,\delta}$ versus δ. (c) $q_{95}^{chease}/q_{95}^{new,no\,\epsilon}$ versus ϵ. (d) $q_{95}^{chease}/q_{95}^{new,no\,\delta\epsilon}$ versus $\delta\epsilon$. (e) $q_{95}^{chease}/q_{95}^{new,no\,w_{07}}$ versus w_{07} (fits with ±5%).

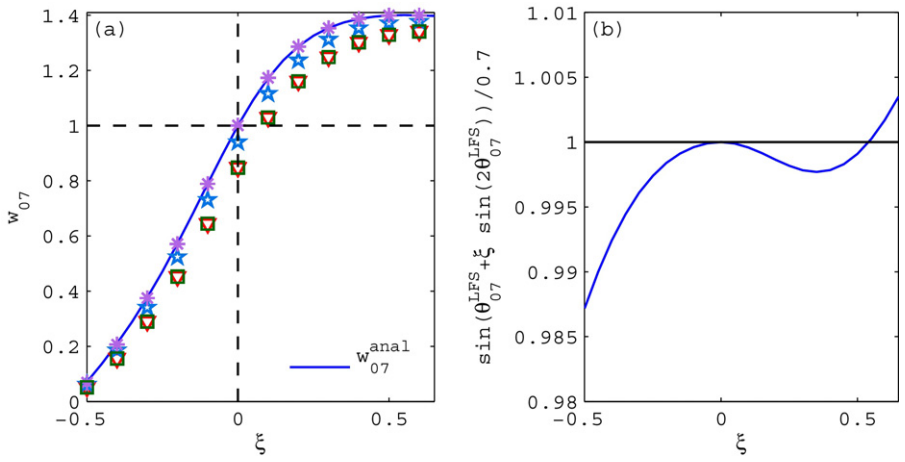

Fig. C22. (a) Symbols: w_{07} and ξ for shapes defined by Eqs. (1) and (2) and with $1<\kappa<3$, $-0.8<\delta<0.8$ and $-0.5<\xi<0.65$. The solid line, $w_{07}^{anal,\delta\sim0}$ from Eq. (C.3) using Eq. (C.2), follows the $\delta=0$ points. (b) $\sin[\theta_{LFS}^{07}+\xi\sin 2\theta_{LFS}^{07}]/0.7$ with θ_{LFS}^{07} from Eq. (C.2).

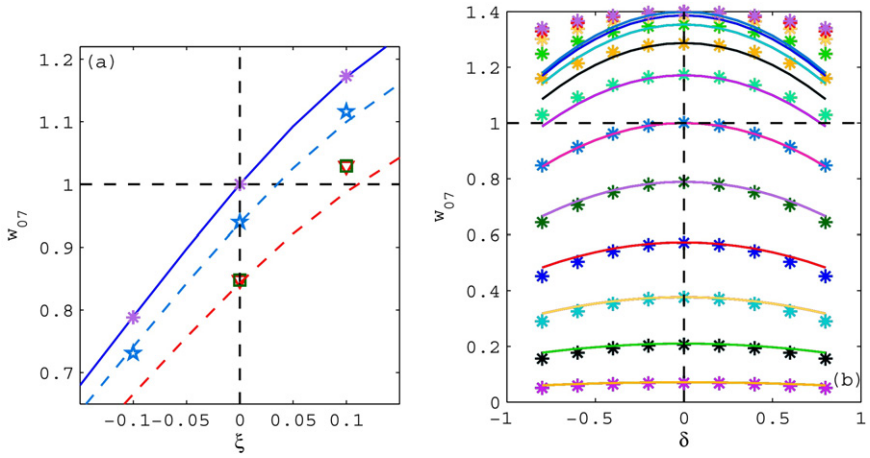

Fig. C23. (a) Zoom of Fig. C22(a), adding dashed lines from w_{07}^{anal}, Eq. (C.5), with $\delta=\pm0.5$ and ±0.8. (b) w_{07} versus triangularity for various values of ξ between -0.5 and 0.6 by steps of 0.1. Symbols from actual plasma boundaries as in Fig. C22 and solid lines from Eq. (C.5) using Eq. (C.2).

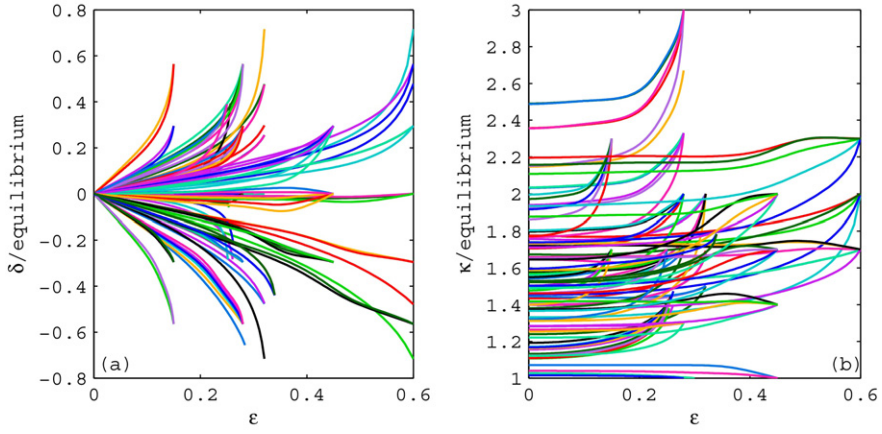

Fig. D24. δ and κ profiles versus "minor radius", with ϵ the local inverse aspect ratio of the respective flux surface, for each equilibria shown in Fig. 1.

References

[1] M. Kikuchi, et al., Negative triangularity tokamak as fusion energy system, in: Conf. Proc 1st Int. e-Conf. on Energies, 2014 http://sciforum.net/conference/ece-1.
[2] S. Yu. Medvedev, et al., The negative triangularity tokamak: stability limits and prospects as a fusion energy system, Nucl. Fusion 55 (2015) 06301.
[3] C.G. Petty, et al., Feasibility study of a compact ignition tokamak based upon gyroBohm scaling physics, Fusion Sci. Technol. 43 (2003) 1.
[4] Z. Dragojlovic, A.R. Raffray, F. Najmabadi, et al., An advanced computational algorithm for systems analysis of tokamak power plants, Fusion Eng. Des. 85 (2010) 243.
[5] J. Johner, HELIOS: a zero-dimensional tool for next step and reactor studies, Fusion Sci. Technol. 59 (2011) 308.

[6] M. Kovari, R. Kemp, H. Lux, P. Knight, J. Morris, D.J. Ward, PROCESS: a system code for fusion power plants—Part 1: Physics, Fusion Eng. Des. 89 (2014) 3054.
[7] H. Lütjens, A. Bondeson, O. Sauter, The CHEASE code for toroidal MHD equilibria, Comput. Phys. Commun. 97 (1996) 219.
[8] N.A. UCKAN, ITER Physics Group, ITER Physics Design Guidelines: 1989, IAEA/ITER/DS-10, IAEA, Vienna, 1990.
[9] N.A. UCKAN, ITER Physics Group, ITER physics design guidelines, Fusion Sci. Technol. 19 (1991) 1493.
[10] T. Stoltzfus-Dueck, et al., X-point-position-dependent intrinsic toroidal rotation in the edge of the TCV tokamak, Phys. Rev. Lett. 114 (2015) 245001.
[11] T. Stoltzfus-Dueck, et al., X-point position dependence of edge intrinsic toroidal rotation on the Tokamak á configuration variable, Phys. Plasmas 22 (2015) 056118.
[12] O. Sauter, S. Yu, Medvedev Tokamak coordinate conventions: COCOS, Comput. Phys. Commun. 184 (2013) 293.
[13] S. Ramanujan, Ramanujan's Collected Works, Chelsea, New York, 1962.
[14] O. Sauter, C. Angioni, Y.R. Lin-Liu, Neoclassical conductivity and bootstrap current formulas for general axisymmetric equilibria and arbitrary collisionality regime, Phys. Plasmas 6 (1999) 2834, O. Sauter, C. Angioni, Y.R. Lin-Liu, Neoclassical conductivity and bootstrap current formulas for general axisymmetric equilibria and arbitrary collisionality regime, Phys. Plasmas 9 (2002) 5140.
[15] O. Sauter, et al., Marginal beta limit for NTM in JET H-mode discharges, Plasma Phys. Control. Fusion 44 (2002) 1999.
[16] O. Sauter, A simple formula for the trapped fraction in tokamaks including the effect of triangularity, Lausanne Report LRP 01/2013. http://infoscience.epfl.ch/record/187521.
[17] M. Raghunathan, et al., Simulation of bootstrap current in 2D and 3D ideal magnetic fields in tokamaks, Nucl. Fusion (2016) (in press).